





Two-dimensional arrays of Bose-Einstein condensates: Interference and stochastic collapse dynamics

Youjia Huang ¹, Shu Nagata,² Joseph Jachinowski ², Jiazhong Hu ^{3,1,4,*} and Cheng Chin ^{2,†}

¹*Department of Physics and State Key Laboratory of Low Dimensional Quantum Physics, Tsinghua University, Beijing 100084, China*

²*James Franck Institute, Enrico Fermi Institute, and Department of Physics, University of Chicago, Chicago, Illinois 60637, USA*

³*Beijing Academy of Quantum Information Science, Beijing 100193, China*

⁴*Frontier Science Center for Quantum Information and Collaborative Innovation Center of Quantum Matter, Beijing 100084, China*



(Received 12 May 2024; revised 15 October 2024; accepted 19 November 2024; published 13 December 2024)

We demonstrate two-dimensional arrays of Bose-Einstein condensates (BECs) as a new experimental platform with parallel quantum simulation capability. A defect-free array of up to 49 BECs is formed by loading a single BEC with 50 000 atoms into 7×7 optical wells. Each BEC is prepared with independent phases, confirmed by matterwave interference. Based on BEC arrays, we realize fast determination of the phase boundary of BECs with attractive interactions. We also observe the stochastic collapse dynamics from the distribution of atom numbers in the array. We show that the collapse of a BEC can occur much faster than the averaged decay of an ensemble. The BEC arrays enable new forms of experiments to drastically increase the measurement throughput and to quantum simulate, say, large 2D Josephson-junction arrays.

DOI: [10.1103/PhysRevResearch.6.043272](https://doi.org/10.1103/PhysRevResearch.6.043272)

I. INTRODUCTION

Optical tweezer arrays have emerged as a new exciting platform to realize independent control of individual atoms, enabling experiments on atomic qubits for applications in quantum information and quantum metrology [1–5]. This contrasts the optical lattice platform, which does not offer easy control over individual atoms, but has the advantage of keeping a large number of atoms in the quantum degenerate regime [6].

To combine the strengths of both platforms, innovative ideas have been investigated to employ the concept of optical tweezers to manipulate multiple quantum degenerate ensembles [7–9]. One approach is to prepare an array of Bose-Einstein condensates (BECs) by loading a single BEC into multiple optical or magnetic potential wells [10,11]. Based on a few BECs in a 1D chain, quantum simulation of Josephson-junctions has been realized [12–15]. Quantum simulation of a 2D Josephson-junction array has also been proposed based on a 2D array of BECs [16]. In addition, each BEC in the array is envisaged as a quantum memory unit [17–19]. Finally, since the cycle of the BEC experiment is typically long, preparation of many BECs in an array can significantly improve the experimental throughput and statistics.

In this paper, we demonstrate a two-dimensional (2D) array of up to 7×7 BECs in a single experiment. This is realized by adiabatically loading a single atomic BEC into

a 2D array of optical wells, each supporting a small BEC. By interfering the BECs in the array, we show that the BECs after the transfer possess independent phases. We use the 2D array to realize parallel experiments to quickly determine the stability phase diagram of BECs with attractive interactions. By directly comparing BECs in the array, we show that the collapse dynamics of a BEC is stochastic in nature.

II. EXPERIMENTAL SETUP

We start the experiment by preparing a BEC of 5×10^4 cesium atoms at the scattering length $a = 200a_0$, where a_0 is the Bohr radius. In the vertical direction, the BEC is tightly confined to a single site of an optical lattice with trap frequency $\omega_z = 2\pi \times 400$ Hz. In the horizontal directions, the BEC is weakly confined by a flat-bottomed square potential well with a side length of 50 μm and barrier height $h \times 370$ Hz, where $h = 2\pi\hbar$ is the Planck constant. The optical potential is formed by projecting a blue-detuned light at 788 nm with a digital micromirror device (DMD), see Fig. 1(a) and details in Appendix A.

We divide the initial BEC into an array of M^2 small BECs by adiabatically loading the BEC into an $M \times M$ array of potential wells formed by the DMD. The separation between adjacent wells is $d = 11.7, 8.4, 5.8 \mu\text{m}$ for $M = 4, 5,$ and 7 , respectively. The depth of the potential well is $h \times 20$ to $h \times 80$ Hz, calculated from the trap frequency measurement. The barrier between two BECs can be precisely controlled by the laser intensity, for which we achieved stability $>99.98\%$ based on servo control with a low-noise, high speed photodetector. When the barrier is much higher than the chemical potential, tunneling between neighboring BECs is exponentially suppressed and the BECs are isolated. Experiments described in this paper proceed in this regime. Tunneling becomes strong and the tunneling energy is much less sensitive

*Contact author: hujiazhong01@ultracold.cn

†Contact author: cchin@uchicago.edu

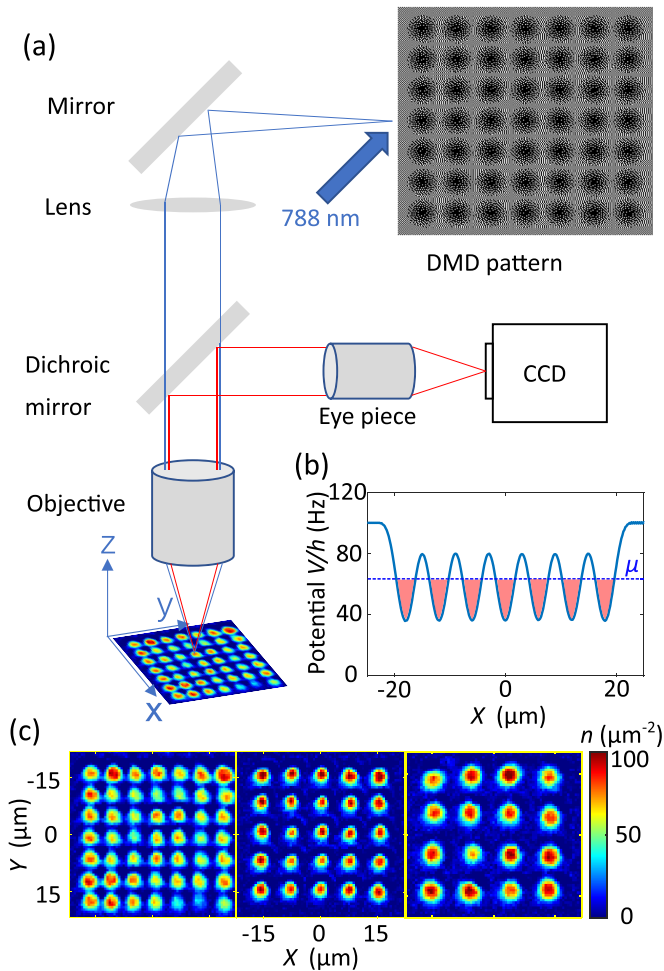


FIG. 1. Experimental preparation of two-dimensional (2D) arrays of BECs. (a) A digital micromirror device (DMD) is placed at the image plane of the atomic sample. A 788 nm beam illuminates the DMD, which projects the desired intensity pattern on the atoms. A pattern based on 341×341 micromirrors is shown, which generates 7×7 optical wells. Here bright pixels correspond to the micromirrors that reflect the light to the atoms; dark pixels correspond to the micromirrors that do not. (b) A 1D line cut of seven optical potential wells on the atom plane. We raise the barriers between the wells higher than the chemical potential μ to separate individual BECs. (c) Images of 2D array with 7×7 , 5×5 , and 4×4 BECs. Each site contains 1000 \sim 2000 atoms. The color represents the atomic density.

to the intensity instability when the barrier is low, which is a beneficial condition to simulate Josephson junction array.

To ensure adiabaticity, the blue-detuned light is slowly turned on in 200 ms and the scattering length is simultaneously ramped to a small final value of $a_f < 20 a_0$ using a Feshbach resonance [20]. This procedure reduces the chemical potential and isolates each BEC in a single well, see Fig. 1(b). After loading, we perform *in situ* or time-of-flight (TOF) imaging on the atoms to confirm the preparation process, see examples in Fig. 1(c).

III. INTERFERENCE OF THE BEC ARRAY

To verify that the initial BEC is converted into M^2 separate BECs, we interfere them from different wells in a TOF

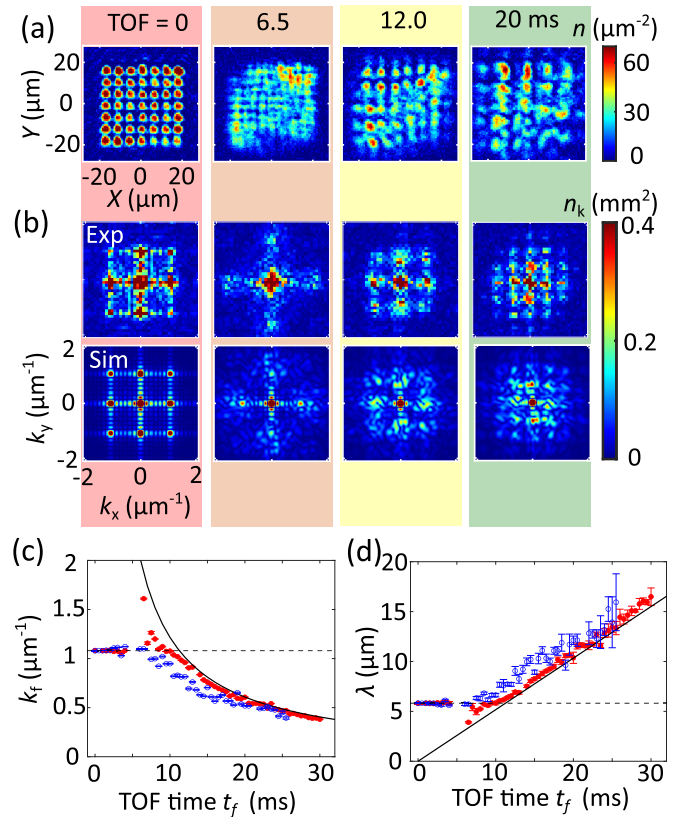


FIG. 2. Interference of a two-dimensional array of BECs. (a) Images of 49 BECs during the time-of-flight expansion. Here atomic scattering length is $a_f = 3 a_0$. (b) Fourier transform of the atomic density profile (upper). Numerical simulation under the same condition (lower). (c) The wave vector k_f of the main side peaks in the Fourier spectrum. Red circles are data taken at $a_f = 3 a_0$; Blue circles are data taken at $a_f = 75 a_0$. The dashed line indicates the initial BEC separation of $5.8 \mu\text{m}$. The solid line indicates the predicted interference wave vector $k_f = md/\hbar t_f$. (d) The period of density modulation extracted from the Fourier transform. The dashed line is the separation between optical wells. The solid line is the predicted spacing $\lambda = \hbar t_f/md$. Error bars show one standard deviation.

experiment. Interference of two BECs [21–23] and 1D BEC array [24–26] were studied previously. The fringe period due to two interfering BECs is $\lambda = \hbar t_f/md$ where t_f is the TOF time and m is the atomic mass. The same fringe spacing is observed for 1D BEC arrays with random phases [24].

We implement the interference experiment with a BEC loaded into 7×7 optical wells. We quickly remove all horizontal confinement, which allows the atoms from different wells to freely expand, see Fig. 2. Clear density waves appear when the expanding BECs overlap, see Fig. 2(a). To determine the periodicity of the waves, we Fourier transform the atomic density distribution and extract the dominant nonzero wavenumber k_f in the momentum space (see Appendix B). The result and the associated period $\lambda = 2\pi/k_f$ are shown in Figs. 2(b)–2(d).

For short expansion times $t_f \leq 5$ ms, there is insufficient overlap of BECs from different wells. Thus, the period of the density variation is simply given by the separation of optical wells $d = 5.8 \mu\text{m}$. For $t_f > 6$ ms, the interference pattern emerges with a spatial period λ which increases with

time, consistent with the theoretical prediction. Repeating the experiment with the atomic scattering length tuned to $a_f = 3$ and $75 a_0$ right before the TOF, we observe a slightly longer period for $75 a_0$.

The appearance of matter interference confirms the preparation of a 2D BEC array. We further investigate the phase coherence of the BECs in different wells by comparing our experimental results to numerical simulation of the Gross-Pitaevskii equation (GPE). In the simulation we find that if the phases of the BECs are identical, the potential well spacing d persists as the dominant length scale over hundreds of ms; in contrast, if the phases of the BECs are random, the initial periodicity d is rapidly replaced by the interference fringe spacing (see Appendix B). In our experiment, the initial periodicity d only persists in the first 5 ms, and the interference fringes spacing become dominant afterwards. Our result is fully consistent with independent BECs prepared with random matterwave phases.

In fact, we are working in the regime by splitting micro-BECs with negligible tunneling. The uncertainty principle $\Delta N \Delta \phi \geq 1$ suggests that in the absence of particle exchange ($\Delta N < 1$), the relative phase becomes undefined $\Delta \phi \gg \pi$. This resembles the loss of matterwave coherence when the BEC enters a Mott insulator phase in deep optical lattices, where phase coherence between neighboring sites is lost. Our demonstration of parallel experiments were performed in this regime. If we want to maintain the coherence, we may apply a weaker DMD potential such that neighboring BECs remain connected to allow particle exchange corresponding to $\Delta N \gg 1$. This is equivalent to the superfluidity phase in an optical lattice. Such control is feasible by reducing the intensity of the laser that forms the DMD potential.

IV. PARALLEL EXPERIMENTS BASED ON THE BEC ARRAY

An intriguing application of BEC arrays is to perform parallel experiments. One experimental cycle on a $M \times M$ BEC array yields M^2 measurements and thus increases the data throughput. In addition, BECs can be prepared in different conditions, which allow us to directly compare many systems under an otherwise identical environment. Such parallel experiments are less sensitive to systematics than the standard repetitive experiments.

We demonstrate the power of parallel experiments with BEC arrays by investigating the stability phase boundary of BECs with negative scattering length $a < 0$. Collapse of a BEC occurs when the atomic attraction or the atomic density exceeds a critical value. BEC collapse has been studied in former experiments [27–34]. The stability condition is theoretically calculated to be $-a/\ell < 0.574/N$ [35], where $\ell = \sqrt{\hbar/m\bar{\omega}}$ is the harmonic length of the trap and $\bar{\omega}$ is the geometric mean of the trap frequencies.

To determine the phase boundary, an array of 4×4 BECs with initial scattering length $4 a_0$ is employed. We increase the BEC separation to $8.4 \mu\text{m}$ and the potential barrier between them to 4 nK to ensure the independent evolution of each BEC. The scattering length is then quickly quenched to different negative values $a_f < 0$. After a hold time t_h , we image the BECs and see if they have collapsed.

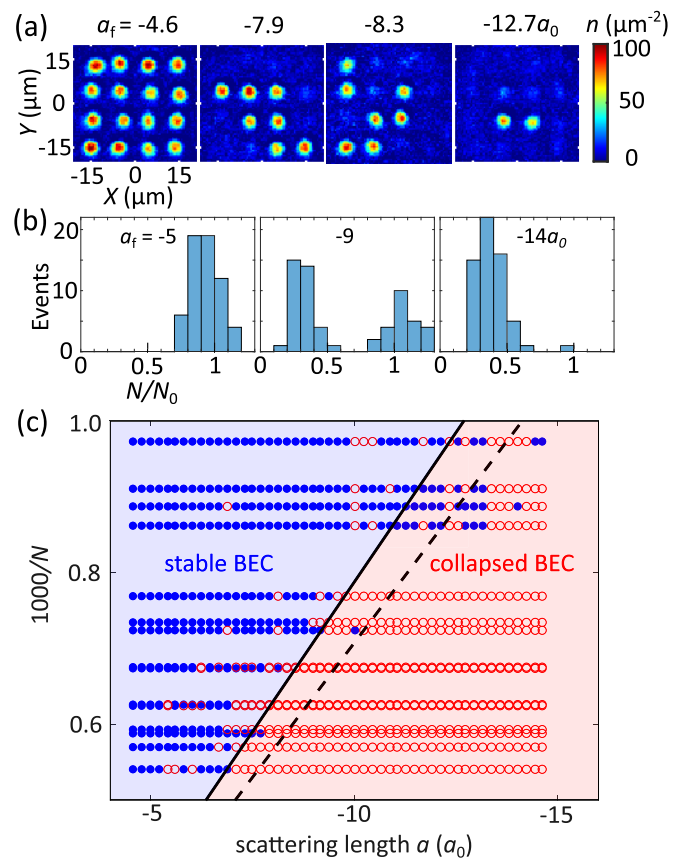


FIG. 3. Collapse of BECs in a 2D array with attractive interactions. (a) Images of BEC arrays after a hold time of $t_h = 50$ ms. The atomic population quickly drops when BEC collapses. The trap frequencies approximately $(\omega_x, \omega_y, \omega_z) = 2\pi \times (15, 15, 400)$ Hz. (b) Histograms of remaining atom number N normalized to the atom number N_0 at $a_f = -4.6 a_0$. (c) Stability phase diagram of BEC with attractions constructed based on 2D arrays of BECs with different initial atom numbers N and scattering lengths a_f . Blue filled circles are stable BECs and red open circles are collapsed BECs. Dashed line shows the predicted critical scattering length $a_c = -0.574\ell/N$. Solid line is a fit to the data which yields $a_c = -0.51(7)\ell/N$. See details in Appendix C.

In situ imaging clearly distinguishes collapsed and stable BECs after a hold time $t_h = 50$ ms, see Fig. 3(a). In stable BECs, the atom number remains essentially unchanged, while the atom number drops sharply to $20 \sim 40\%$ in the collapsed BECs. The dichotomy of stable and collapsed BEC manifests in the histogram of the remaining atom number, see Fig. 3(b). Similar histograms have also been observed in [34]. The histogram shows two distinct peaks at 100% and 35% of the initial number. In very few cases do we see BECs with an atom number falling between $60 \sim 80\%$. Thus, we introduce the threshold fraction of 70% , below (above) which the BEC is considered collapsed (stable).

The 16 BECs in the array allow us to efficiently determine the phase boundary between stable and collapsed BECs for various initial particle numbers and scattering lengths. We start the experiment with an array of 4×4 BECs, where each BEC is prepared with a different atom number between 1000 and 2000 by slight tuning of the trap depth of each well. We verify that the initial population is reproducible to better than

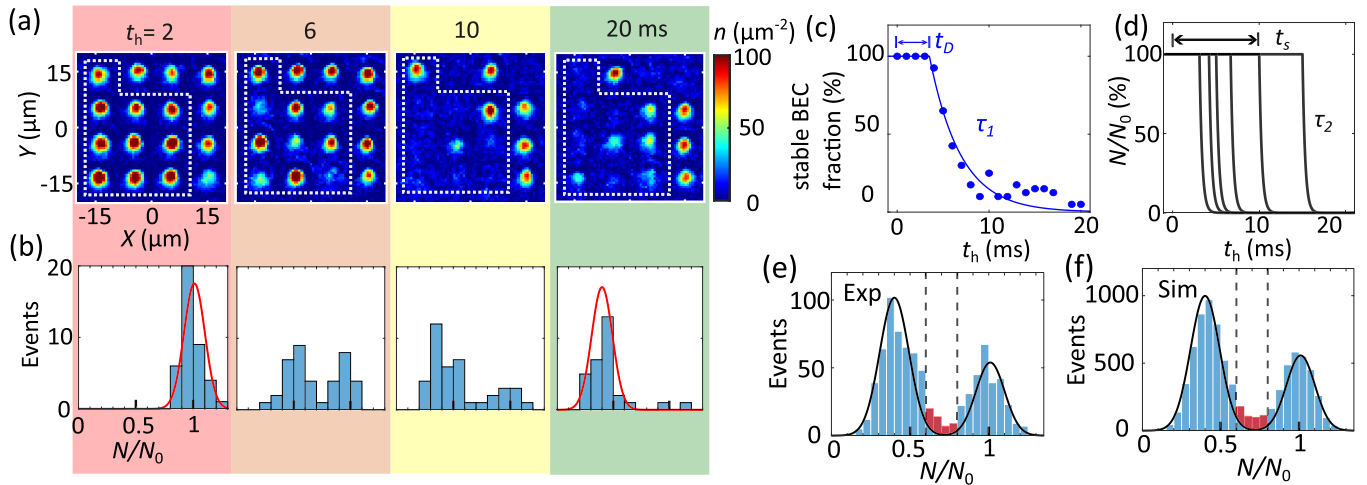


FIG. 4. Stochastic collapse of BECs with attractive interactions. (a) An array of 16 BECs with scattering length quenched to $a_f = -9 a_0$. We build statistics based on samples with similar initial atom numbers (within 10%), enclosed by the white dashed line. (b) Histograms of normalized atom numbers $n \equiv N/N_0$ based on four repeated experiments. Gaussian fit to the histogram at $t_h = 2$ ms gives the mean $\bar{n} = 1.0$ and standard deviation $\sigma = 0.09$ for stable BECs, and the fit to histogram at $t_h = 20$ ms gives $\bar{n} = 0.4$ and $\sigma = 0.09$ for the collapsed BECs. (c) Averaged BEC survival fraction, taking 70% as threshold, remains unity for $t_D = 3.5(4)$ ms after the quench (see Appendix D). Then decay occurs with a time constant of $\tau_1 = 3.4(5)$ ms. Blue line shows an empirical fit. (d) Illustration of our statistical model, where each BEC is stable for a stochastic time t_s , followed by the collapse that occurs within a $1/e$ time of τ_2 (black lines). (e) Histogram of atom number of all 810 samples with 0 to 20 ms hold time. Black lines are fits based on the stable and collapsed BEC distributions from panel (b). The red parts of the histogram are excess events of BECs with intermediate atom number $0.6 \leq \bar{n} < 0.8$. (f) Histogram from the theory model based on 8100 samples. By comparing data and the model, we determine the collapse process of a single BEC takes $\tau_2 = 1.3(2)$ ms.

90%. The nonuniform preparation of the BECs tests the dependence of the BEC stability on the atom number. Repeating the experiment for different scattering lengths a_f , we see a clear boundary between stable and unstable BECs. Our result shows that the critical scattering length a_c reduces for BECs with more atoms, consistent with the theoretical prediction $a_c/\ell = -\kappa/N$, where $\kappa = 0.574$ [35]. An independent fit to our data yields $\kappa = 0.51(7)$, see Fig. 3. Our result is consistent with the former measurement of $\kappa = 0.46(6)$ [33] and the theoretical prediction within our measurement uncertainty.

Near the boundary between stable and collapsed BECs, we observe unusually large fluctuations in the remaining atom number. This, together with the double-peak structure in the histogram, suggests that the collapse is likely a highly stochastic process. This scenario has been discussed in Ref. [28]. To better understand the collapse process, we prepare a 4×4 BEC array with almost identical initial atom numbers at scattering length $-1 a_0$. We then quickly quench the scattering length near the phase boundary at $a_f = -9 a_0 = -0.5 \ell/N$ and monitor their evolution. We build statistics of the atom number based on ten of the 16 sites whose initial atom numbers are stable and close to each other, see Figs. 4(a) and 4(b). The variation in particle number is mainly due to the finite size of the laser beam generating the optical potential. A laser beam with a finite size imposes a weaker optical potential away from the beam center and thus reduces the atom number and, to a lesser extent, the particle number stability of micro-BECs far from the center. This issue is solvable with a stronger laser beam with a larger beam size or a laser beam engineered to have a uniform intensity profile. After $t_h = 4$ ms, BECs start collapsing and we again observe two peaks in the histogram, indicating some BECs remain stable while some have fully

collapsed. After 20 ms, almost all BECs have collapsed. Based on 810 samples, an ensemble average of the survival fractions shows that BECs remain stable for a delay time of $t_D = 3.5(4)$ ms and then collapse occurs with an averaged $1/e$ lifetime of $\tau_1 = 3.4(5)$ ms, see Fig. 4(c).

During the collapse process, the two-peak structure in the histogram persists. The rarity of events between the two peaks suggests that the collapse dynamics proceeds very quickly. Thus, almost all BECs are found to be either stable or fully collapsed. In other words, few BECs are recorded in the middle of the collapse process. This is analogous to the radiative decay of heavy elements, where the half-life can be much longer than the time scale of the nuclear reaction.

We construct a stochastic model to describe the decay of metastable BECs with attractive interactions. After quenching the magnetic field, we assume each BEC takes a duration of t_D to reach the atomic density that is high enough to initiate the collapse process. This observation is consistent with previous works [34,36,37] and is explained by the development of modulation instability [37,38]. The collapse then occurs stochastically with a time constant of τ_1 .

We introduce a microscopic time scale τ_2 in the model to characterize the duration of the collapse process of a single BEC. To extract τ_2 , we numerically calculate the histogram for different τ_2 and compare with the measurement (see Appendix D). We focus on the events falling between the two peaks in the histogram for the atom number between $60 \sim 80\%$ and show that among 810 BEC samples in the 2D arrays, less than 5% of the events are between the two peaks that cannot be accounted for by the initial and collapsed BEC atom number distributions. The events falling in this range indicate the BECs that are in the middle of the collapse

process. These events are marked red in Figs. 4(e) and 4(f). The scarcity of these events indicates that collapse in a BEC occurs so fast that one can hardly capture the BECs in the decay process. By comparing with the numerical model (see Appendix D), we determine the microscope collapse time scale to be $\tau_2 = 1.3(2)$ ms.

The stable time $t_D = 3.5(4)$ ms and the decay time of $\tau_1 = 3.4(5)$ ms suggest that the BECs can remain stable for approximately 7 ms. Once the collapse occurs, however, the BEC decays rapidly within 1.3(2) ms. This picture is illustrated in Fig. 4(d).

In the mean field picture, the metastability of BECs with small attraction comes from the quantum pressure that balances the attraction [39]. When the attraction approaches the critical value $a_f \rightarrow a_c$, however, stochastic collapse of the BECs can occur due to the suppressed kinetic energy barrier, which can be overcome by thermal or quantum fluctuations of the BECs. Our picture also explains the observation in the ^{85}Rb BEC experiment [36], where the averaged collapse dynamics is found to be much slower than the theory expectation [40]. This is because the averaged lifetime of metastable BECs can be much longer than the microscopic time scale to collapse a single BEC.

V. CONCLUSION

In summary, we demonstrate three forms of experiments with 2D BEC arrays. First, matterwave interference of 49 BECs shows that the each BEC acquires an independent phase. Second, when each BEC is prepared differently, we realize fast mapping of the phase diagram. Finally, parallel experiments on arrays of BECs with attractive interactions reveal the stochastic nature of the collapse. Collapse of a single BEC can occur much faster than the ensemble-averaged decay.

The new forms of parallel experiments to quickly extract phase diagrams and to reveal the stochastic decay of attractive BECs highlight the unique strength and potential of the BEC array as a new quantum simulation platform. Each micro-BEC in the array may also serve as a memory unit for scalable quantum information processing. Additionally, each BEC can serve as an atom interferometer for detection of acceleration and rotation [41]. Compared to using lattices, a DMD device

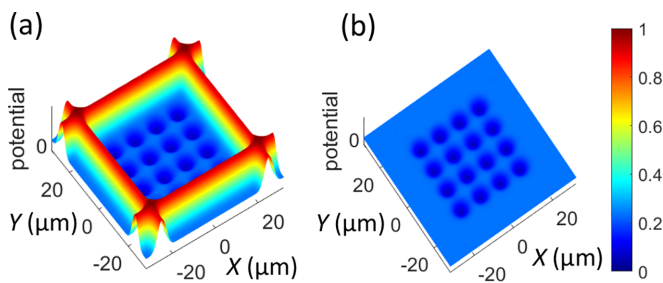


FIG. 5. Optical potentials for trapping initial single BEC (a) and an array of M^2 BECs (b). (a) Initially, a single BEC with high chemical potential is confined by four walls generated by the DMD. (b) After reducing the scattering length, the BEC is converted into an array of smaller BECs, each confined by the optical wells.

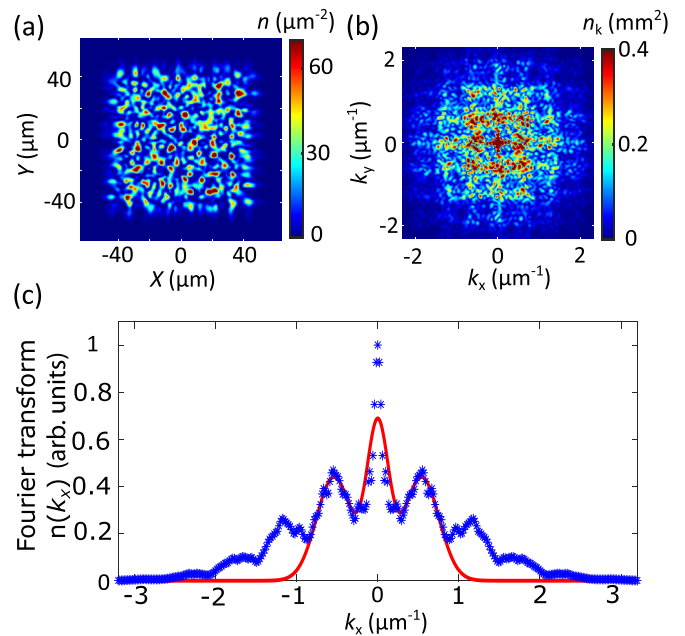


FIG. 6. Determination of the density profile periodicity. (a) Simulated 2D density in real space of a BEC sample after 20 ms TOF. (b) Fourier transform of the simulated 2D density from (a). (c) Integrated Fourier transform in the k_y direction (blue dots). Fitting the central peak and two side peaks (red line) yields the density periodicity.

offers greater flexibility: the spacing between two sites is more adjustable, site resolution can be easily achieved with a standard objective, and the potential of individual wells can be tuned independently. With sufficient atoms in a BEC, our scheme can be easily generalized to prepare 100 to 1000 BECs in a single experiment. Such quantum gas array platform will invite more innovations in research on quantum simulation and quantum information processing.

ACKNOWLEDGMENTS

This work is supported by National Science Foundation under Grants No. PHY-1511696 and No. PHY-2103542. Y.H. and J.H. acknowledge support from the National Key Research and Development Program of China (No. 2021YFA0718303 and No. 2021YFA1400904), National Natural Science Foundation of China (No. 92165203, No. 92476110, No. 61975092, and No. 11974202), and Tsinghua University Initiative Scientific Research Program. S.N. acknowledges support from the Takenaka Scholarship Foundation.

APPENDIX A: PREPARATION OF A TWO-DIMENSIONAL (2D) ARRAY OF BOSE-EINSTEIN CONDENSATES (BECs)

Our experiment begins by preparing approximately 5×10^4 atoms in a three-dimensional BEC at the scattering length $a = 200 a_0$, where a_0 is the Bohr radius. Then, we gradually turn on a DMD potential with shallow 2D wells and a repulsive square boundary in 200 ms [Fig. 5(a)]. Next, we turn on a vertical lattice to transfer the BEC into a single lattice site in 600 ms. At the same time, we ramp down the scattering

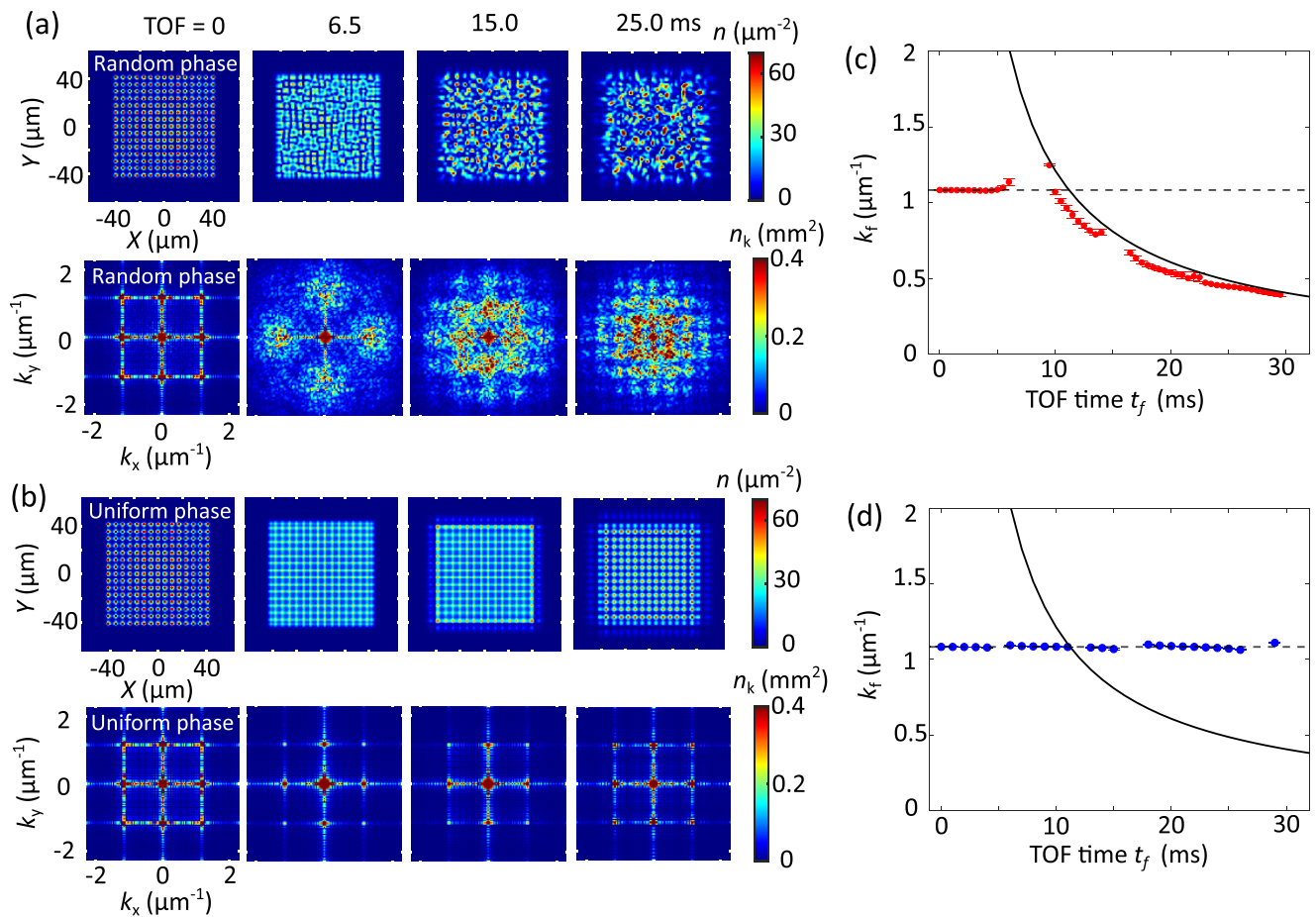


FIG. 7. Gross-Pitaevskii equation(GPE) simulation of interference in a BEC array with random and constant relative phases. (a) Time evolution of a 2D array of BECs in free space, where the phases of the BECs in different sites are random. (b) Time evolution of a 2D array of BECs in free space, where the phases of the BECs are constant. (c) The wave vector k_f corresponds to the main side peaks in the Fourier spectrum (as described in the main text). Red circles correspond to BECs with random phases, following $k_f = md/\hbar t_f$, as indicated by the solid line. (d) Blue circles correspond to BECs with constant phases, following the initial BEC separation, as indicated by the dashed line.

length to $a = 20 a_0$ in 300 ms. As scattering length decreases, the chemical potential drops, causing the atoms to settle into the shallow wells. Next, we switch the DMD pattern to turn off the repulsive square boundary [Fig. 5(b)], allowing the hot atoms to escape. Finally, we tune the scattering length a to an even lower value ($4 a_0$ for experiments in Fig. 3 and $-1 a_0$ for experiments in Fig. 4) before proceeding to the experiments described in main text.

APPENDIX B: DETERMINATION OF FRINGE PERIOD AND GROSS-PITAEVSKII EQUATION(GPE) SIMULATION

First, we perform a Fourier transform on the density profile to obtain the atomic distribution in reciprocal space [Figs. 6(a) and 6(b)]. Since the system is symmetrical in the k_x and k_y directions, we sum over the k_y direction to obtain the integrated 1D density profile [Fig. 6(c)] and extract the period in the k_x direction. We determine the density periodicity from the positions of the dominant side peaks in the momentum space. To obtain the positions of the side peaks at $k_x = \pm k_f$, we simultaneously fit the central peak and the two side peaks using a sum of three Gaussians [Fig. 6(c)].

We utilize GPELab [42,43], which is based on the Gross-Pitaevskii equation (GPE), to simulate the experiment. To speed up the calculation, we assume the system is a 2D gas confined in the x - y plane, rather than conducting a 3D simulation. In the z direction, the system is in the ground state of a harmonic trap with a trap frequency of $2\pi \times 400$ Hz. We use the simulation scheme *Relaxation* as described in Ref. [43] to evolve the system from $t_s = 0$ to 30 ms. The time step for the simulation is set to 0.005 ms. At $t_s = 0$ ms, the sample is released into free space. The spatial range in both the x and y directions spans from -160 to $160 \mu\text{m}$, and the space grid is defined with a size of 513×513 . The initial wave function consists of a 15×15 BEC array with each site containing 800 atoms. The distance between neighboring sites is $d = 5.8 \mu\text{m}$. In Fig. 7(a), the phases of different sites are set to random value, whereas in Fig. 7(b) they are set to be uniform. As the number of sites in the array increases, the interference pattern for a random phase case becomes more obvious, which is consistent with the result in 1D arrays [24].

The time-evolution results are presented in Fig. 7. When the initial relative phases are random, an interference pattern emerges after a few ms of evolution, as shown in Fig. 7(a).

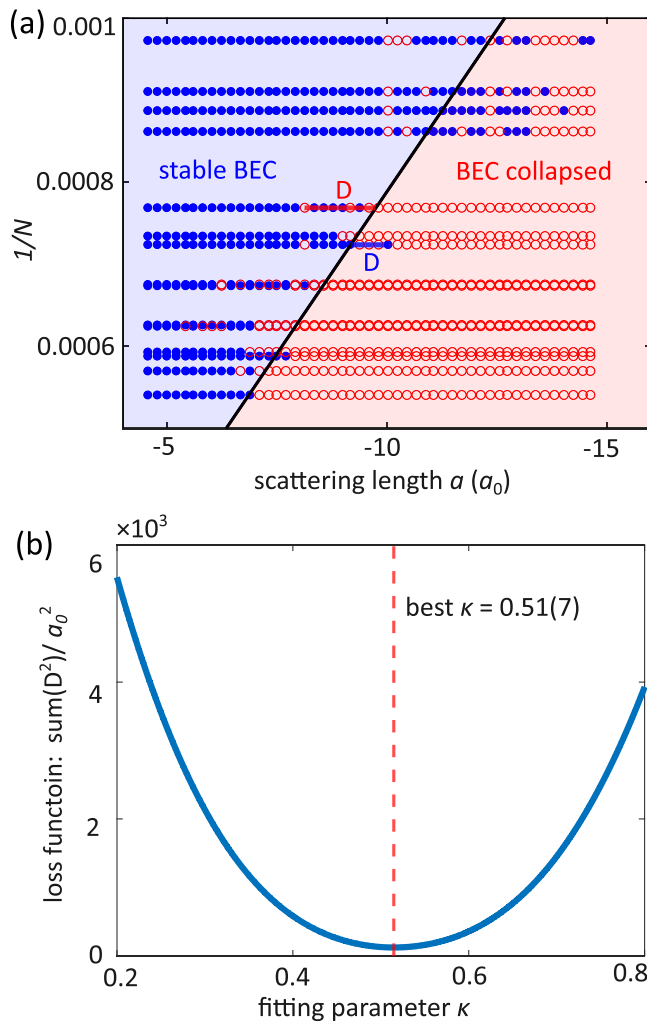


FIG. 8. Determination of the fitting constant κ . (a) If a data point lies on the incorrect side of the boundary, as defined by Eq. (C1), for example, red circles to the left of the solid line and blue circles to the right of the solid line, we calculate the distance D from such a point to the boundary. The loss function is then calculated by summing distances for all such data points. (b) The variation of the loss function with κ is shown, where the loss function reaches its minimum at $\kappa = 0.51(7)$, as indicated by the dashed line.

The periodicity of the interference pattern is more clear in reciprocal space, as evidenced by the bottom row of Fig. 7(a). Thus, we determine the periodicity in Fourier space. The simulated k_f for the case of random phases approximately follows the solid line in Fig. 7(c), given by $\lambda = \hbar t_f/md$, with $\lambda = 2\pi/k_f$. This simulation result is consistent with our experiment observations.

On the other hand, if the initial phases of BECs are uniform, the periodicity remains constant throughout an evolution time of 30 ms, as depicted in Fig. 7(b). This result indicates that the period of the density is preserved by the initial period over an extended duration. The simulated k_f for the case of uniform phases does not match our experimental

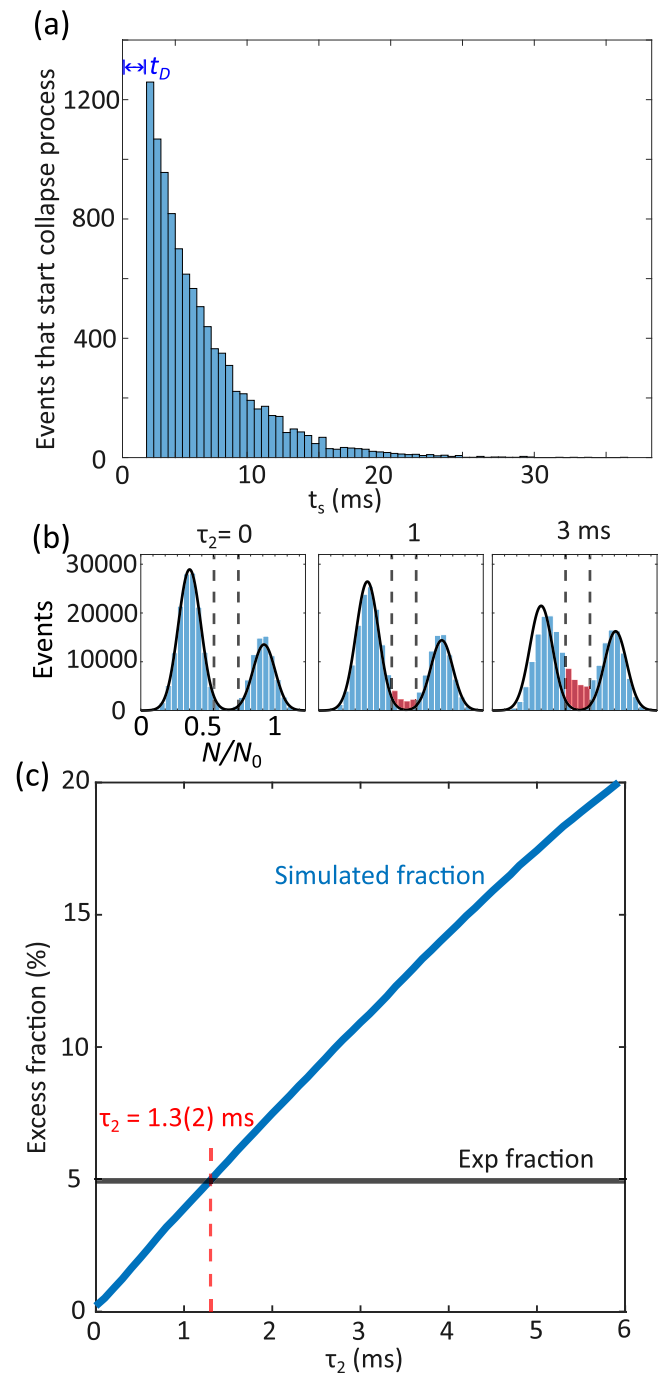


FIG. 9. Determination of τ_2 through simulation. (a) Events that initiate the collapse process from 100%. (b) The histogram depicts the atom numbers obtained from simulations. Black lines are fits based on the distributions of stable and collapsed BECs. The red parts of the histogram represent the excess of events of BECs with intermediate atom numbers in the range $0.6 < \bar{n} < 0.8$. (c) The fraction of excess events. The blue line represents the change in the residual fraction as a function of τ_2 . The black line marks the position of the residual fraction from our experiment data, and the red dashed line corresponds to $\tau_2 = 1.3(2)$ ms determined from the simulation.

observations. Therefore, we conclude that the BEC samples in our experiment have random phases.

APPENDIX C: DETERMINATION OF THE BOUNDARY BETWEEN STABLE AND COLLAPSED BEC

On the boundary of noncollapsed and collapsed samples, the reciprocal of the atom number $1/N$ is expected to be proportional to the negative scattering length a_c . Our task is to determine the proportionality constant κ , such that

$$a_c/\ell = -\kappa/N, \quad (\text{C1})$$

where a_c denotes the critical scattering length at which the BEC collapses with atom number N , $\ell = \sqrt{\hbar/m\bar{\omega}}$ represents the harmonic oscillator length of the trap, and $\bar{\omega}$ denotes the geometric mean of the trap frequencies.

Based on the experiment data shown in Fig. 3, we use the least squares method to determine the optimal value of κ . The first step is to define a loss function. For a given parameter κ , we could draw a line l_κ . We assume that the samples to the left of this line correspond to noncollapsed samples [depicted as blue dots in Fig. 8(a)] and those to the right to collapsed samples [depicted as red circles in Fig. 8(a)]. If a data point is misclassified, such as a red circle falling on the left side, it is considered an error point. We measure the horizontal distance D [as depicted in Fig. 8(a)] from the error points to the line l_κ , and the sum of squares of these D is computed as the loss. We plot the loss as a function of κ [Fig. 8(b)], and determine the optimal κ value that minimizes the loss function. Our result of $\kappa = 0.51(7)$ is reported in the main text.

APPENDIX D: STOCHASTIC MODEL OF BEC COLLAPSE AND SIMULATIONS TO DETERMINE t_D AND τ_2

As detailed in the main text, our stochastic model is composed of two steps. In the first step, as the instability of BEC grows, the atom number remains constant for a duration t_s , which we treat as a random variable. In the second step, the BEC begins to collapse, resulting in an exponential decrease in the atom number, characterized by a time constant τ_2 .

From the experiment, we know that the probability distribution function (PDF) of the random variable $t_D = 3.5(4)$ ms is composed of two parts. Initially, as the modulation instability requires time $t_D = 3.5(4)$ ms to develop [37], for $t_s < t_D$, the probability of collapse is zero. Subsequently, after t_D , the probability of collapse would decrease with a time constant of $\tau_1 = 3.4(5)$ ms. Utilizing this PDF, we could generate 10 000 samples of t_s [Fig. 9(a)].

For the simplicity in the simulation, we use normalized atom numbers. The initial atom number N_0 is set to 1. After one BEC fully collapsed, approximately 40% of atoms remain. For a given sample, after a time evolution t_h , if $t_h \leq t_s$, the atom number N_t remains unchanged. If $t_h > t_s$, N_t will decay to $e^{-(t_h-t_s)/\tau_2} \times (1 - 0.4) + 0.4$.

Additionally, beyond this idealized process, there is fluctuation in the atom number due to imperfections in loading. We model this fluctuation as a Gaussian distribution with a standard deviation $\sigma = 0.09$. This statistical variation is then added to the atom number to obtain the final atom number N_t . We set t_h to range from 0 ms to 20 ms with a spacing of 1 ms.

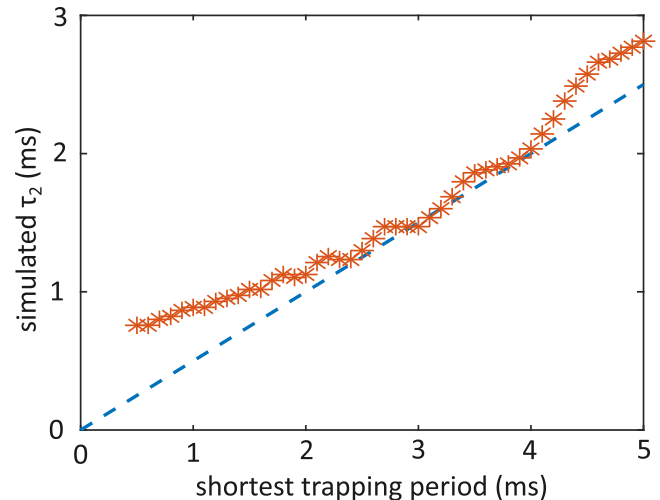


FIG. 10. Dependence of τ_2 on the shortest trapping period. Stars indicate simulated results based on the GPE, and the dashed line represents the condition where τ_2 equal to half of the shortest trapping period. We find that simulated results do not always align with the dashed line.

Subsequently, we obtain the histogram of all events at all time t_h [Fig. 9(b)].

From the experiment, we observe that the atom numbers of noncollapsed and collapsed samples follow two Gaussian distributions, each with a relative standard deviation $\sigma = 0.09$, and mean values centered at 1 and 0.4, respectively, as depicted by black solid lines in Fig. 4(b). Therefore, we fit the histogram with Gaussian distributions to represent the distributions of noncollapsed and collapsed samples. There would be excess parts, particularly between 60% to 80% [Fig. 9(b), and Figs. 4(e) and 4(f)]. We treat the residual part as samples that are in the middle of the process of losing particles, and calculate the fraction of such residual samples as a function of τ_2 [Fig. 9(c)]. In the experiment, this fraction is measured

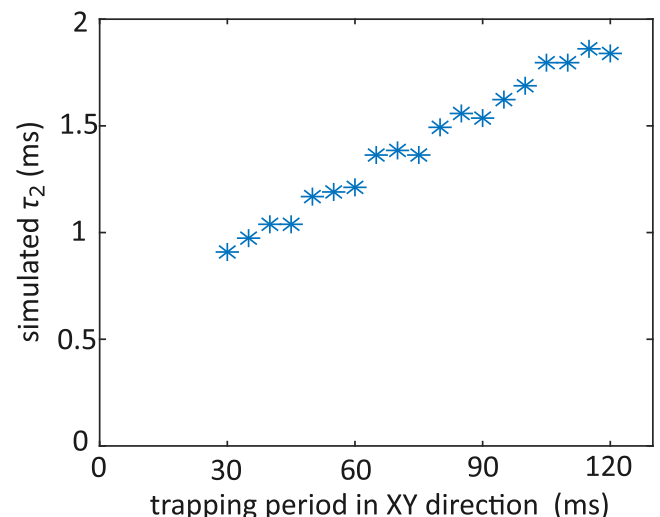


FIG. 11. Dependence of τ_2 on the trapping period in the loose (x and y) directions. Stars indicate simulated results. When the trapping periods in the loose (x and y) directions become shorter, τ_2 is also smaller.

to be 4.9%. Based on this measurement, we determine the optimal value of τ_2 that matches this fraction to be 1.3(2) ms. We also apply different threshold values of 62.5% \sim 77.5% and 65% \sim 75% and obtain $\tau_2 = 1.1$ ms and 1.2 ms, respectively. These values are consistent with the result of 1.3(2) ms in the main text, and confirm that the estimation of τ_2 is insensitive to the range of our choice. Based on the time scale given in Ref. [37], we find that the 10% fluctuation in the initial number of atom N would lead to an approximately 4% uncertainty in t_D and τ_1 , which is within the uncertainty from our fitting.

During the experiments, we linearly ramp the scattering length from $-a_0$ to the phase boundary $-9a_0$ within 1 \sim 2 ms, which is short compared to delay time t_D and τ_1 . Since the modulation instability would start only when the scattering length reaches the critical scattering length, the finite ramp speed would only very slightly extend t_D and does not affect the estimation of τ_1 and τ_2 .

In Refs. [40,44–48], the Gross-Pitaevskii equation (GPE) with a three-body loss term is used to simulate the collapse process. We also apply this method to our system. With the current trapping period and a three-body loss coefficient of 7×10^{-28} cm⁶/s, the decay time is calculated to be $\tau_2 = 1.3$ ms. By maintaining the trapping periods in the x and y directions and varying the shortest trapping period (z direction), we observed that τ_2 is not always exactly half of the shortest trapping period (Fig. 10). Furthermore, we set the shortest trapping period to be 2.5 ms and vary the trapping period in the loose directions (x and y) from 30 ms to 120 ms. Based on the simulation, we found that τ_2 also depends on the trapping period in the x and y directions (Fig. 11).

In general, a smaller trapping period results in a higher initial density. The cloud accumulates at the bottom of the trap more rapidly and reaches a larger density. The higher initial density and faster dynamics contribute to a more rapid three-body loss and a smaller τ_2 .

-
- [1] A. M. Kaufman and K.-K. Ni, Quantum science with optical tweezer arrays of ultracold atoms and molecules, *Nat. Phys.* **17**, 1324 (2021).
- [2] G. Tóth and I. Apellaniz, Quantum metrology from a quantum information science perspective, *J. Phys. A: Math. Theor.* **47**, 424006 (2014).
- [3] X. Zhang and J. Ye, Precision measurement and frequency metrology with ultracold atoms, *Natl. Sci. Rev.* **3**, 189 (2016).
- [4] M. F. Riedel, P. Böhi, Y. Li, T. W. Hänsch, A. Sinatra, and P. Treutlein, Atom-chip-based generation of entanglement for quantum metrology, *Nature (London)* **464**, 1170 (2010).
- [5] L. Pezze, A. Smerzi, M. K. Oberthaler, R. Schmied, and P. Treutlein, Quantum metrology with nonclassical states of atomic ensembles, *Rev. Mod. Phys.* **90**, 035005 (2018).
- [6] I. Bloch, J. Dalibard, and W. Zwerger, Many-body physics with ultracold gases, *Rev. Mod. Phys.* **80**, 885 (2008).
- [7] Y. Wang, S. Shevate, T. M. Wintermantel, M. Morgado, G. Lochead, and S. Whitlock, Preparation of hundreds of microscopic atomic ensembles in optical tweezer arrays, *npj Quantum Inf.* **6**, 54 (2020).
- [8] J. Trisnadi, M. Zhang, L. Weiss, and C. Chin, Design and construction of a quantum matter synthesizer, *Rev. Sci. Instrum.* **93**, 083203 (2022).
- [9] A. W. Young, W. J. Eckner, N. Schine, A. M. Childs, and A. M. Kaufman, Tweezer-programmable 2D quantum walks in a Hubbard-regime lattice, *Science* **377**, 885 (2022).
- [10] L. Fallani, C. Fort, J. E. Lye, and M. Inguscio, Bose-Einstein condensate in an optical lattice with tunable spacing: transport and static properties, *Opt. Express* **13**, 4303 (2005).
- [11] S. Jose, P. Surendran, Y. Wang, I. Herrera, L. Krzemien, S. Whitlock, R. McLean, A. Sidorov, and P. Hannaford, Periodic array of Bose-Einstein condensates in a magnetic lattice, *Phys. Rev. A* **89**, 051602 (2014).
- [12] F. S. Cataliotti, S. Burger, C. Fort, P. Maddaloni, F. Minardi, A. Trombettoni, A. Smerzi, and M. Inguscio, Josephson junction arrays with Bose-Einstein condensates, *Science* **293**, 843 (2001).
- [13] R. Gati, M. Albiez, J. Foelling, B. Hemmerling, and M. K. Oberthaler, Realization of a single Josephson junction for Bose-Einstein condensates, *Appl. Phys. B* **82**, 207 (2006).
- [14] R. Gati and M. K. Oberthaler, A bosonic Josephson junction, *J. Phys. B: At. Mol. Opt. Phys.* **40**, R61 (2007).
- [15] B. P. Anderson and M. A. Kasevich, Macroscopic quantum interference from atomic tunnel arrays, *Science* **282**, 1686 (1998).
- [16] T. Kopeć and M. Bogdan, Berezinskii-Kosterlitz-Thouless transition in two-dimensional arrays of Josephson coupled Bose-Einstein condensates, *Phys. Lett. A* **377**, 2581 (2013).
- [17] L.-M. Duan, M. D. Lukin, J. I. Cirac, and P. Zoller, Long-distance quantum communication with atomic ensembles and linear optics, *Nature (London)* **414**, 413 (2001).
- [18] Y. Colombe, T. Steinmetz, G. Dubois, F. Linke, D. Hunger, and J. Reichel, Strong atom-field coupling for Bose-Einstein condensates in an optical cavity on a chip, *Nature (London)* **450**, 272 (2007).
- [19] S. Riedl, M. Lettner, C. Vo, S. Baur, G. Rempe, and S. Dürr, Bose-Einstein condensate as a quantum memory for a photonic polarization qubit, *Phys. Rev. A* **85**, 022318 (2012).
- [20] C. Chin, R. Grimm, P. Julienne, and E. Tiesinga, Feshbach resonances in ultracold gases, *Rev. Mod. Phys.* **82**, 1225 (2010).
- [21] M. Andrews, C. Townsend, H.-J. Miesner, D. Durfee, D. Kurn, and W. Ketterle, Observation of interference between two Bose condensates, *Science* **275**, 637 (1997).
- [22] A. Röhrl, M. Naraschewski, A. Schenzle, and H. Wallis, Transition from phase locking to the interference of independent Bose condensates: Theory versus experiment, *Phys. Rev. Lett.* **78**, 4143 (1997).
- [23] Y. Shin, M. Saba, T. A. Pasquini, W. Ketterle, D. E. Pritchard, and A. E. Leanhardt, Atom interferometry with Bose-Einstein condensates in a double-well potential, *Phys. Rev. Lett.* **92**, 050405 (2004).
- [24] Z. Hadzibabic, S. Stock, B. Battelier, V. Bretin, and J. Dalibard, Interference of an array of independent Bose-Einstein condensates, *Phys. Rev. Lett.* **93**, 180403 (2004).

- [25] M. Gustavsson, E. Haller, M. J. Mark, J. G. Danzl, R. Hart, A. J. Daley, and H.-C. Nägerl, Interference of interacting matter waves, *New J. Phys.* **12**, 065029 (2010).
- [26] P. Pedri, L. Pitaevskii, S. Stringari, C. Fort, S. Burger, F. S. Cataliotti, P. Maddaloni, F. Minardi, and M. Inguscio, Expansion of a coherent array of Bose-Einstein condensates, *Phys. Rev. Lett.* **87**, 220401 (2001).
- [27] C. C. Bradley, C. A. Sackett, and R. G. Hulet, Bose-Einstein condensation of lithium: Observation of limited condensate number, *Phys. Rev. Lett.* **78**, 985 (1997).
- [28] C. A. Sackett, H. T. C. Stoof, and R. G. Hulet, Growth and collapse of a Bose-Einstein condensate with attractive interactions, *Phys. Rev. Lett.* **80**, 2031 (1998).
- [29] R. A. Duine and H. T. C. Stoof, Stochastic dynamics of a trapped Bose-Einstein condensate, *Phys. Rev. A* **65**, 013603 (2001).
- [30] Y. Kagan, A. E. Muryshev, and G. V. Shlyapnikov, Collapse and Bose-Einstein condensation in a trapped Bose gas with negative scattering length, *Phys. Rev. Lett.* **81**, 933 (1998).
- [31] V. M. Perez-Garcia, H. Michinel, J. I. Cirac, M. Lewenstein, and P. Zoller, Dynamics of Bose-Einstein condensates: Variational solutions of the Gross-Pitaevskii equations, *Phys. Rev. A* **56**, 1424 (1997).
- [32] C. Huepe, S. Metens, G. Dewel, P. Borckmans, and M.-E. Brachet, Decay rates in attractive Bose-Einstein condensates, *Phys. Rev. Lett.* **82**, 1616 (1999).
- [33] J. L. Roberts, N. R. Claussen, S. L. Cornish, E. A. Donley, E. A. Cornell, and C. E. Wieman, Controlled collapse of a Bose-Einstein condensate, *Phys. Rev. Lett.* **86**, 4211 (2001).
- [34] C. Eigen, A. L. Gaunt, A. Suleymanzade, N. Navon, Z. Hadzibabic, and R. P. Smith, Observation of weak collapse in a Bose-Einstein condensate, *Phys. Rev. X* **6**, 041058 (2016).
- [35] M. Houbiers and H. Stoof, Stability of Bose condensed atomic ^7Li , *Phys. Rev. A* **54**, 5055 (1996).
- [36] E. A. Donley, N. R. Claussen, S. L. Cornish, J. L. Roberts, E. A. Cornell, and C. E. Wieman, Dynamics of collapsing and exploding Bose-Einstein condensates, *Nature (London)* **412**, 295 (2001).
- [37] J. H. V. Nguyen, D. Luo, and R. G. Hulet, Formation of matter-wave soliton trains by modulational instability, *Science* **356**, 422 (2017).
- [38] P. J. Everitt, M. A. Sooriyabandara, M. Guasoni, P. B. Wigley, C. H. Wei, G. D. McDonald, K. S. Hardman, P. Manju, J. D. Close, C. C. N. Kuhn *et al.*, Observation of a modulational instability in Bose-Einstein condensates, *Phys. Rev. A* **96**, 041601 (2017).
- [39] C. J. Pethick and H. Smith, *Bose-Einstein Condensation in Dilute Gases* (Cambridge university press, Cambridge, 2008).
- [40] S. Wüster, B. J. Dabrowska-Wüster, A. S. Bradley, M. J. Davis, P. B. Blakie, J. J. Hope, and C. M. Savage, Quantum depletion of collapsing Bose-Einstein condensates, *Phys. Rev. A* **75**, 043611 (2007).
- [41] K. Stolzenberg, C. Struckmann, S. Bode, R. Li, A. Herbst, V. Vollenkemper, D. Thomas, E. M. Rasel, N. Gaaloul, and D. Schlippert, Multi-axis inertial sensing with 2D arrays of matter waves, [arXiv:2403.08762](https://arxiv.org/abs/2403.08762).
- [42] X. Antoine and R. Duboscq, GPELab, a Matlab toolbox to solve Gross-Pitaevskii equations I: Computation of stationary solutions, *Comput. Phys. Commun.* **185**, 2969 (2014).
- [43] X. Antoine and R. Duboscq, GPELab, a Matlab toolbox to solve Gross-Pitaevskii equations II: Dynamics and stochastic simulations, *Comput. Phys. Commun.* **193**, 95 (2015).
- [44] H. Saito and M. Ueda, Mean-field analysis of collapsing and exploding Bose-Einstein condensates, *Phys. Rev. A* **65**, 033624 (2002).
- [45] L. Santos and G. V. Shlyapnikov, Collapse dynamics of trapped Bose-Einstein condensates, *Phys. Rev. A* **66**, 011602 (2002).
- [46] C. M. Savage, N. P. Robins, and J. J. Hope, Bose-Einstein condensate collapse: A comparison between theory and experiment, *Phys. Rev. A* **67**, 014304 (2003).
- [47] S. K. Adhikari, Dynamics of collapsing and exploding Bose-Einstein condensate, *Phys. Lett. A* **296**, 145 (2002).
- [48] P. A. Altin, G. R. Dennis, G. D. McDonald, D. Doering, J. E. Debs, J. D. Close, C. M. Savage, and N. P. Robins, Collapse and three-body loss in a ^{85}Rb Bose-Einstein condensate, *Phys. Rev. A* **84**, 033632 (2011).